

The very early optical afterglow of GRBs, revealing the nature of the ejecta

Y. Z. Fan

*Department of Physics, University of Nevada, Las Vegas NV 89154, USA
Purple Mountain Observatory, Chinese Academy of Science, Nanjing 210008, China. and
National Astronomical Observatories, Chinese Academy of Sciences, Beijing, 100012, China.*

Bing Zhang

Department of Physics, University of Nevada, Las Vegas NV 89154, USA

D. M. Wei

*Purple Mountain Observatory, Chinese Academy of Science, Nanjing 210008, China. and
National Astronomical Observatories, Chinese Academy of Sciences, Beijing, 100012, China.*

We show that if the GRB ejecta itself is magnetized or neutron-rich, the very early afterglow of GRBs is very different from that powered by a pure ion fireball. In the *Swift* era, with the well monitored early afterglow data, we can potentially diagnose the ejecta composition and reveal the nature of the central GRB engine.

I. INTRODUCTION

Since the discovery of the optical flash of GRB 990123 [1], great attention has been paid to the very early optical afterglow (e.g., for theory see [5, 17, 18, 19, 21, 25, 26, 29, 31, 33]; for observation, see [2, 13, 14, 16, 22, 28]) of soft, long GRBs. The very early optical afterglow of short GRBs and X-ray flashes have also been investigated in some detail [8, 11].

In nearly all these theoretical papers, the fireballs are assumed to be non-magnetized and neutron-free. However, in principle, the ejecta may be significantly magnetized (see [23] and the references therein) or contain a large amount of neutrons (e.g. [3, 6]), or both (e.g. [30]). Recently we have studied the early afterglow emission (especially the reverse shock emission) of a magnetized ejecta and a neutron-rich ejecta [9, 12, 32]. Here we summarize the main results. Comparing these results with the early afterglow observations, we may get insight into the initial composition of the outflow and reveal the nature of the central engine.

II. REVERSE SHOCK EMISSION FROM MAGNETIZED EJECTA

A. Magnetized reverse shock emission from GRB 990123 and GRB 021211

A bright optical flash was detected during the bright GRB 990123 (e.g., [1]). The peak V-band flux was 8.9th magnitude. After the peak, the flux drops as t_{obs}^{-2} (before the peak, the flux increases as $t_{\text{obs}}^{3.1}$). Such a sharp decrease has been modeled by the emission from the shocked electrons contained in the reverse shock region with adiabatic cooling [25, 29]. With a more careful investigation, Fan et al. found that

by taking the reverse shock model and the physical parameters found in modeling the multi-wavelength afterglow from the forward shock emission, the theoretical peak flux of the optical flash accounts for only 3×10^{-4} of the observed value ($\sim 1\text{Jy}$) [7]. In order to remove this discrepancy, they suggested that the electron and magnetic equipartition parameters, ϵ_e and ϵ_B , should be 0.61 and 0.39, respectively. These are much different from the corresponding values for the late afterglow (~ 0.1 and ~ 0.001).

In a more general discussion, Zhang, Kobayashi & Mészáros introduced a parameter \mathcal{R}_B (which is defined as $(\epsilon_B^r/\epsilon_B^f)^{1/2}$; where the superscripts r and f represent the reverse shock region and forward shock region, respectively) to trace the magnetization of the GRB outflows [33]. They found $\mathcal{R}_B \sim 15$ for GRB 990123 and $\mathcal{R}_B > 1$ for GRB 021211.

These results have been also confirmed in several more detailed analysis of both bursts [20, 24, 27]. As a result, it is quite robust to say that the reverse shock region is magnetized, at least for GRB 990123 and GRB 021211. In the following, we introduce a parameter σ , the ratio between the electromagnetic energy flux and the particle energy flux, to describe the initial magnetization of the outflow (we assume that the magnetic field is ordered).

B. Reverse shock emission with mild magnetization

As the outflow interacts with the surrounding medium, two shocks form. One is the forward shock expanding into the medium, and the other is the reverse shock penetrating into the outflow. The forward shock jump condition is the same as that of a pure hydrodynamical fireball model [4], but the reverse shock jump condition is different (see equations (2-5) of [10] for the general form).

The novel features include: **1.** At the reverse shock front, for $\sigma > 0.01$, the amplified ordered magnetic field (B_{ord}) is significantly stronger than that of the random one (B_{ran}). In the ISM medium, the typical synchrotron radiation $\nu_m \propto B_{\text{ord}}$ is much lower than $\nu_R \sim 4.6 \times 10^{14} \text{ Hz}$ and the reverse shock-accelerated electrons are in the slow cooling regime. The observed flux scales as

$$F_\nu \propto B_{\text{ord}} \nu_m^{(p-1)/2} \propto B_{\text{ord}}^{(p+1)/2}. \quad (1)$$

Therefore, the R-band reverse shock emission is stronger for a higher B_{ord} (see Fig.1), which matches the observation of GRB 990123 and GRB 021211. However, for $\sigma > 0.1$, the reverse shock is suppressed (in both [9] and [32], the ideal MHD approximation is taken. If magnetic dissipation [10] is taken into account, the result would be different), so that the reverse shock peak level starts to decrease (see Fig.1). In the wind medium case, the R-band reverse shock emission with magnetization is weaker (see Fig. 2) since the reverse shock is relativistic and the electrons are in the fast cooling phase, and ν_m is above ν_R . The observed flux scales as

$$F_\nu \propto B_{\text{ord}} \nu_c^{1/2} \propto B_{\text{ord}}^{-1/2}, \quad (2)$$

where $\nu_c \propto B^{-3}$ is the cooling frequency. As a result, F_ν decreases with increasing σ .

2. In the very early afterglow phase, the outflow is ultrarelativistic. Due to the beaming effect, the area we view is very narrow where the orientation of magnetic field is nearly the same. The local high linear polarization can not be averaged effectively. As a result, net high linear polarization is expected. By introducing a parameter $b = B_{\text{ord}}/B_{\text{ran}}$, the net linear polarization can be approximated by (e.g., [9])

$$\Pi_{\text{net}} \approx 0.60 \frac{b^2}{1 + b^2}. \quad (3)$$

Even for $\sigma \sim 0.01 - 0.1$, the linear polarization as high as 30% is expected.

C. The reverse shock emission with arbitrary magnetization

Zhang & Kobayashi have performed a detailed analytical investigation on the reverse shock emission with arbitrary magnetization [32]. For $\sigma < 1$, i.e., the mildly magnetized regime, their results are rather similar to that of [9]. For $\sigma > 1$, i.e., the high- σ regime, it is found out that the reverse shock peak is broadened, mainly due to the separation of the shock crossing radius and the deceleration radius of the outflow (see Fig.3). This novel feature can be regarded as a signature of high σ .

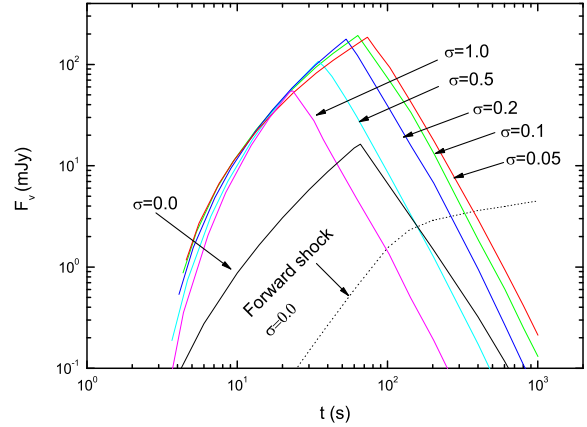


FIG. 1: The very early R-band ($\nu_R = 4.6 \times 10^{14} \text{ Hz}$) light curve powered by the mildly magnetized outflow (the degrees of the magnetization have been marked in the figure) interacting with the interstellar medium. The parameters taken in the calculation are: $z = 1$, $E_{\text{kin}} = 10^{53} \text{ ergs}$, $L = 2 \times 10^{51} \text{ ergs s}^{-1}$, $p = 2.2$, $\eta = 300$, $n = 1 \text{ cm}^{-3}$, $\epsilon_e = 0.3$ and the radiation efficiency $\epsilon = \epsilon_e$, where E_{kin} is the total initial energy of the outflow, L is the luminosity of the γ -ray emission, η is the initial bulk Lorentz factor of the outflow, p is the power-law distribution index of the shock-accelerated electrons, and n is the number density of the medium. For $\sigma = 0$ and the forward shock, it is assumed that $\epsilon_B = 0.01$. From ref [9].

Another important result obtained is that the suppression factor of the reverse shock in the strong magnetic field regime is only mild as long as the shock is relativistic, and it saturates in the high- σ regime (see Fig.4). This indicates that strong relativistic shocks still exist in the high- σ limit, which can effectively convert kinetic energy into heat. The overall efficiency of converting jet energy into heat, however, decreases with increasing σ , mainly because the fraction of the kinetic energy in the total energy decreases [32]. These results have been confirmed by Fan, Wei & Zhang both analytically and numerically [10], see their equations (17-18) and figures 1 and 2.

III. VERY EARLY OPTICAL AFTERGLOW LIGHTCURVES OF NEUTRON-FED GRBS

In the rest frame of the ejecta, the free neutron has a mean lifetime $\sim 900 \text{ s}$. The corresponding β -decay radius reads $R_\beta \sim 8 \times 10^{15} \Gamma_{n,2.5} \text{ cm}$ [34], where $\Gamma_n \sim 300$ is the bulk Lorentz factor of the neutrons (below we call it as N-ejecta). In the internal shock phase, the ion-ejecta (I-ejecta) has been decelerated, but the neutrons are not. They move freely into the medium and decay into protons, neutrinos and electrons. These da-

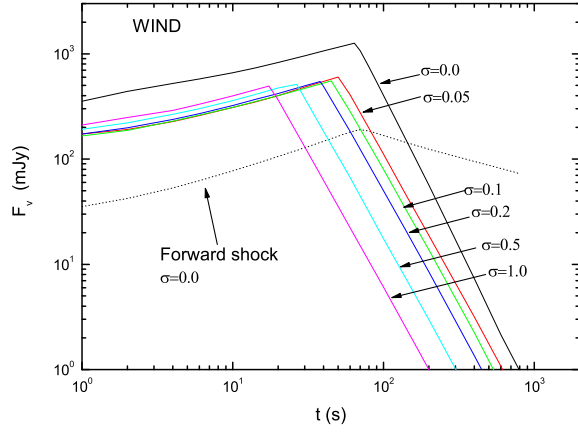


FIG. 2: The very early R-band light curve powered by the mildly magnetized outflow (the degree of the magnetization has been marked in the figure) interacting with a stellar wind. The parameters taken here are the same to those of figure 1 except $n = 3 \times 10^{35} R^{-2} \text{cm}^{-3}$. From ref [9].

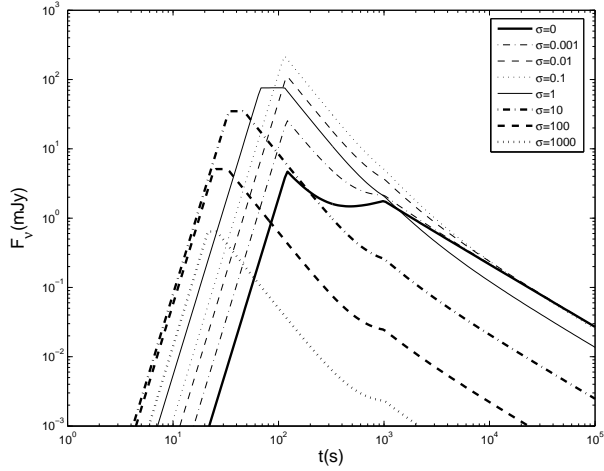


FIG. 3: Sample early afterglow lightcurves for GRBs with an arbitrary magnetization parameter σ . Following parameters are adopted. $E_{\text{kin}} = 10^{52} \text{ergs}$, $T = 20 \text{s}$, $\eta = 150$, $n = 1 \text{cm}^{-3}$, $\epsilon_e^f = \epsilon_e^* = 0.1$, $\epsilon_B^f = 0.001$, $p = 2.2$, and $z = 1$, where T is the duration of the GRB corrected by redshift. Both the forward shock and the reverse shock emission components are calculated and they are superposed to get the final lightcurve. Lightcurves are calculated for different σ values. From ref [32].

cay products share their energy and momentum with the medium and form a mixture (the trail) moving with a bulk Lorentz factor about tens, the actual velocity mainly depends on the density of the medium.

Comparing with that of the pure fireball or the magnetized fireball, the early afterglow of neutron-fed

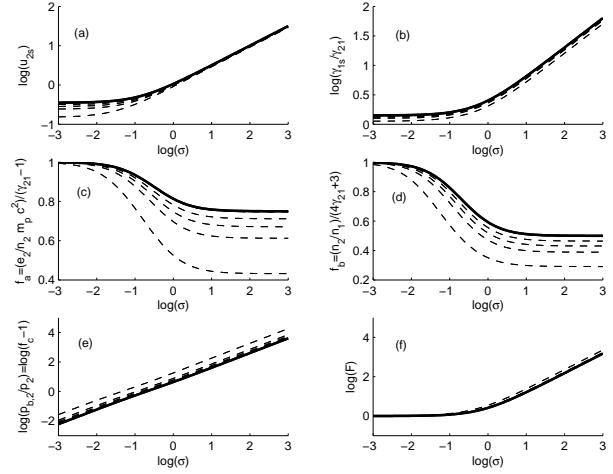


FIG. 4: The variations of six parameters, i.e., u_{2s} , γ_{1s}/γ_{21} , $e_2/n_2 m_p c^2$, n_2/n_1 , $p_{b,2}/p_2$, and F , as a function of σ . The thick solid line is the Kennel-Coroniti solution [15], denoting a $\gamma_{21} \gg 1$ regime. Here u_{2s} is the radial four velocity of region 2 measured in the shock frame; γ_{1s} is the bulk Lorentz factor of region 1 measured in the shock frame; γ_{21} is the Lorentz factor of region 1 relative to region 2; e_2 is the thermal energy density of region 2 (measured in the comoving frame); n_2 (n_1) is the number density of region 2 (1) measured in its comoving frame; $p_{b,2}$ (p_2) is the magnetic field (thermal) pressure of region 2 measured in its comoving frame. The dashed lines, starting from the one closest to the thick line, are for $\gamma_{21} = 1000, 100, 10, 5, 3, 1.5$, respectively. Again the parameters $e_2/n_2 m_p c^2$ and n_2/n_1 are normalized to $(\gamma_{21} - 1)$ and $(4\gamma_{21} + 3)$, respectively. From ref [32].

GRBs is very complicated. The detailed discussion has been presented in [12]. Here we only summarize the main results.

If the medium is a pre-stellar wind, the neutron trail moves slowly, mainly because the medium inertia is too large. The trail and the I-ejecta do not separate from each other, and a forward shock propagates into the trail directly. Three components contribute to the final emission, i.e. the forward shock, the reverse shock propagates into the I-ejecta, and the unshocked trail emission. The latter is significant when χ , the ratio of neutrons to protons, is large, since the internal energy of the unshocked trail is large when the medium density is high. A typical neutron-rich wind-interaction lightcurve is characterized by a prominent early plateau lasting for $\sim 100 \text{s}$ followed by a normal power-law decay (Fig.5). We also show that in the wind case, the IC cooling effect due to the overlapping of the initial prompt γ -ray with the shocks and the trail suppresses the very early R-band afterglow significantly. The neutron-fed signature is also dimmed (see Fig.5(b) and Fig.5(c) for a comparison).

If the medium is a constant density ISM, part of the neutron decay products fall onto the medium, and the trail moves faster than the I-ejecta (In [12], it is as-

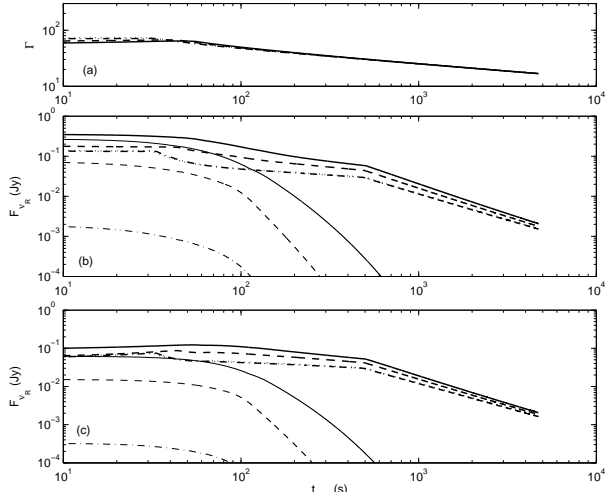


FIG. 5: The early optical afterglow lightcurves of a neutron-fed long GRB in the wind interaction case. (a) The dynamical evolution of the LF of the shocked region as a function of time. (b) R-band lightcurves, with the IC cooling effect due to the prompt γ -rays interacting with the shocked regions being ignored. Thick lines include contributions from all emission components, including the FS, RS and the neutron decay trail. Thin lines are for trail emission only. The dotted, dash-dotted, dashed and solid lines represent $\chi = 0.0, 0.1, 0.5, 1.0$ respectively. Following input parameters are adopted in the calculations: $E_{\text{tot}} = 2.0 \times 10^{53}$ ergs, $\Delta = 10^{12}$ cm, $z = 1$ [i.e. $d_L = 2.2 \times 10^{28}$ cm, which corresponds to the standard $(\Omega_m, \Omega_\Lambda) = (0.3, 0.7)$ Λ CDM cosmological model], $\Gamma_n = 300$, $\Gamma_m = 200$, $\Gamma_{s,n} = 30$, and $n = 10^{35} \text{ cm}^{-3} R^{-2}$ (i.e. $A_* = 1/3$), respectively. The parameters $\epsilon_e = 0.1$, $\epsilon_B = 0.01$ and $p = 2.3$ are adopted for the FS and RS shocks as well as the trail. Where E_{tot} is the total energy of the initial outflow; Δ is the width of the initial I-ejecta; Γ_n ($\Gamma_{s,n}$) is the bulk Lorentz factor of fast (slow) neutrons; Γ_m is the initial bulk Lorentz factor of I-ejecta. (c) R-band lightcurves, but the IC cooling effect due to the prompt γ -rays overlapping with the shocked region and the trail has been taken into account. The averaged γ -ray luminosity is taken as $L_\gamma = 10^{51} \text{ ergs s}^{-1}$. Other parameters and line styles are the same as those in (b). From ref [12].

sumed that the I-ejecta moves slower than the fast neutrons). A gap likely forms between the leading trail and the I-ejecta. The former forms a distinct trail ejecta (T-ejecta) which interacts with the out trail or ISM. The latter catches up later and gives rise to a rebrightening signature. Before collision, the radiation is dominated by the forward shock emission. During the collision, both the forward shock emission and the refreshed shocks (especially the refreshed reverse shock) are important. The unshocked trail emission is not important in this case. A typical neutron-rich ISM-interaction lightcurve is characterized by a slow initial rising lightcurve followed by a prominent bump signature around tens to hundreds of seconds (Fig.6).

For all the cases, the predicted signatures can be

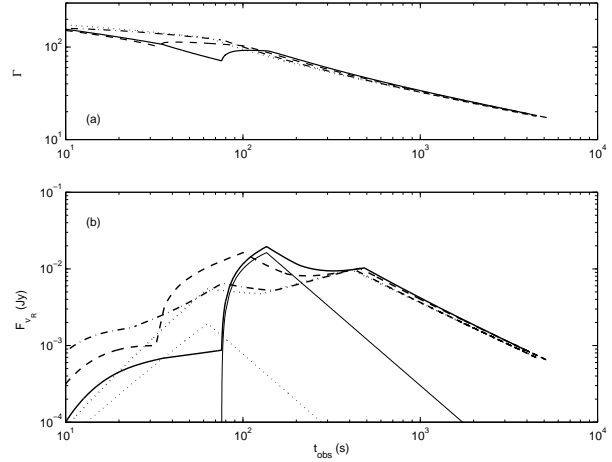


FIG. 6: The early optical afterglow lightcurves of a neutron-fed long GRB in the ISM interaction case. (a) The dynamical evolution of the region shocked by FS as a function of time. The dotted, dash-dotted, dashed, and solid lines represent $\chi = 0.0, 0.1, 0.5, 1.0$ respectively. (b) R-band lightcurves. Line styles are the same as in (a). Thick lines represent the total early R-band lightcurves, while the thin lines are for RS emission only. Only the RS emission for $\chi = 0$ and the RRS emission for $\chi = 1$ cases are plotted. The initial parameters are the same as those listed in the caption of Figure 5, except that $n = 1 \text{ cm}^{-3}$ is adopted. From ref [12].

detected by the UVOT on board the *Swift* observatory. However, most of these signatures (such as the plateau and the bump signature) are not exclusively for neutron decay. More detailed modeling and case study are needed to verify the existence of the neutron component.

IV. DISCUSSION

Most of the current afterglow observations take place hours after the burst trigger. At this stage, the observed afterglow emission are powered by the forward shock, so that essentially all the initial information of the ejecta is lost. In order to diagnose the ejecta composition, well-monitored early afterglow data are needed, since the early afterglow emission, especially in the optical band, is believed to be dominated by the reverse shock emission and possibly the trail emission. The reverse shock propagates into the ejecta, so the emission property, especially the linear polarization degree, depends on the magnetization of the ejecta. The neutron signature emission lasts only tens to hundreds of seconds, which overlaps with the very early shocks emission. Only rapid response to the trigger can catch it.

In this proceedings paper, we have summarized the early afterglow signatures of magnetized GRBs and neutron-rich GRBs. These signatures are likely de-

tectable by the Ultraviolet Optical Telescope (UVOT) on board the *Swift* observatory. Close monitoring of early afterglows from 10s to 1000s of seconds, when combined with detailed theoretical modeling, could be used to diagnose their existence, which may in turn help us to reveal the nature of the GRB central engine source.

Currently, there are just two well studied cases. i.e. GRB 990123, and GRB 021211, whose early afterglow lightcurves are well consistent with reverse shock emission from a moderately-magnetized flow [7, 20, 24, 27, 33]. However, the magnetization itself does not mean the outflow is initially magnetized since in the internal shock phase, random magnetic fields are generated, significant part of which can not be dissipated effectively. These magnetic fields could be retained in the external shock phase to dominate the reverse shock synchrotron emission. In this case,

there is no net polarization expected. Consequently, the early polarization detection is necessary to draw definitive conclusions on the initial magnetization of the ejecta.

Acknowledgments

Y.Z.F thanks the conference organizers for partial support. This work is supported by NASA NNG04GD51G and a NASA Swift GI (Cycle 1) program (for B.Z.), the National Natural Science Foundation (grants 10225314 and 10233010) of China, and the National 973 Project on Fundamental Researches of China (NKBRF G19990754) (for D.M.W.).

-
- [1] Akerlof C. W. et al., 1999, *Nature*, 398, 400
 - [2] Akerlof C. W. et al., 2000, *ApJ*, 532, L25
 - [3] Beloborodov, A. M. 2003, *ApJ*, 588, 931
 - [4] Blandford, R. D., & McKee, C. F. 1976, *Phys. Fluids*, 19, 1130
 - [5] Chevalier, R. A., & Li, Z. Y. 2000, *ApJ*, 536, 195
 - [6] Derishev, D. E., Kocharovsky, V. V., & Kocharovsky, V. V. 1999, *ApJ*, 521, 640
 - [7] Fan, Y. Z., Dai, Z. G., Huang, Y. F., & Lu, T. 2002, *Chin. J. Astron. Astrophys.*, 2, 449 (astro-ph/0306024)
 - [8] Fan, Y. Z., Wei, D. M., & Wang, C. F. 2004, *MNRAS*, 351, L78
 - [9] Fan, Y. Z., Wei, D. M., & Wang, C. F. 2004, *A&A*, 424, 477
 - [10] Fan, Y. Z., Wei, D. M., & Zhang, B. 2004, *MNRAS*, 354, 1031
 - [11] Fan, Y. Z., Zhang, B., Kobayashi, S., & Mészáros, P. 2005, *ApJ* in press (astro-ph/0410060)
 - [12] Fan, Y. Z., Zhang, B., & Wei, D. M. 2005, *ApJ* submitted (astro-ph/0412105)
 - [13] Fox, D. et al. 2003, *Nature*, 422, 284
 - [14] Fox, D. et al. 2003, *ApJ*, 586, L5
 - [15] Kennel, C. F., & Coroniti, F. V. 1984, *ApJ*, 283, 694
 - [16] Kehoe, R., et al. 2000, *ApJ*, 554, L159
 - [17] Kobayashi, S. 2000, *ApJ*, 545, 807
 - [18] Kobayashi, S., & Sari, R. 2000, *ApJ*, 542, 819
 - [19] Kobayashi, S., & Zhang, B. 2003, *ApJ*, 597, 455
 - [20] Kumar, P., & Panaitescu, A. 2003, *MNRAS*, 346, 905
 - [21] Li, Z., Dai, Z. G., Lu, T., & Song, L. M. 2003, *ApJ*, 599, 380
 - [22] Li, W., Filippenko, A.V., Chornock, R. & Jha, S. 2003, *ApJ*, 586, L9
 - [23] Lyutikov, M., & Blandford, R. 2003 (astro-ph/0312347)
 - [24] McMahon, E., Kumar, P., & Panaitescu, A. 2004, *MNRAS*, 354, 915
 - [25] Mészáros, P., Rees, M. J. 1999, *MNRAS*, 306, L39
 - [26] Nakar, E., & Piran, T. 2004, *MNRAS*, 353, 647
 - [27] Panaitescu, A., & Kumar, P. 2004, *MNRAS*, 353, 511
 - [28] Rykoff, E. S. et al. 2004, *ApJ*, 601, 1013
 - [29] Sari, R., & Piran, T., 1999, *ApJ*, 517, L109
 - [30] Vlahakis, N., Peng, F., & Königl. 2003, *ApJ*, 594, L23
 - [31] Wu, X. F., Dai, Z. G., Huang, Y. F., & Lu, T. 2003, *MNRAS*, 342, 1131
 - [32] Zhang, B., & Kobayashi, S. 2005, *ApJ* in press (astro-ph/0404140)
 - [33] Zhang, B., Kobayashi, S., & Mészáros, P. 2003, *ApJ*, 595, 950
 - [34] Through out the paper, the convention $Q_x = Q/10^x$ is taken in cgs units.